



**HAL**  
open science

## Exploring ZnO/Montmorillonite photocatalysts for the removal of hazardous RhB Dye: A combined study using molecular dynamics simulations and experiments

Redouane Haounati, Hamza Ighnih, Rahime Eshaghi Malekshah, Said Alahiane, Fadi Alakhras, Eman Alabbad, Huda Alghamdi, Hassan Ouachtak, Abdelaziz Ait Addi, Amane Jada

### ► To cite this version:

Redouane Haounati, Hamza Ighnih, Rahime Eshaghi Malekshah, Said Alahiane, Fadi Alakhras, et al.. Exploring ZnO/Montmorillonite photocatalysts for the removal of hazardous RhB Dye: A combined study using molecular dynamics simulations and experiments. *Materials Today Communications*, 2023, 35, pp.105915. 10.1016/j.mtcomm.2023.105915 . hal-04297949

**HAL Id: hal-04297949**

**<https://hal.science/hal-04297949v1>**

Submitted on 22 Nov 2023

**HAL** is a multi-disciplinary open access archive for the deposit and dissemination of scientific research documents, whether they are published or not. The documents may come from teaching and research institutions in France or abroad, or from public or private research centers.

L'archive ouverte pluridisciplinaire **HAL**, est destinée au dépôt et à la diffusion de documents scientifiques de niveau recherche, publiés ou non, émanant des établissements d'enseignement et de recherche français ou étrangers, des laboratoires publics ou privés.

# Exploring ZnO/Montmorillonite photocatalysts for the removal of hazardous RhB Dye: A combined study using molecular dynamics simulations and experiments

Redouane Haounati<sup>a,\*</sup>, Hamza Ighnih<sup>a</sup>, Rahime Eshaghi Malekshah<sup>b</sup>, Said Alahiane<sup>c,d</sup>; Fadi Alakhras<sup>e</sup>, Eman Alabbad<sup>f</sup>, Hassan Ouachtak<sup>a, c,\*</sup>, Abdelaziz Ait Addi<sup>a</sup>, Amane Jada<sup>g,h,\*</sup>

<sup>a</sup> Laboratory of Organic and Physical Chemistry, Faculty of Science, Ibn Zohr University, Agadir, Morocco

<sup>b</sup> Medical Biomaterial Research Centre (MBRC), Tehran University of Medical Sciences, Tehran, Iran

<sup>c</sup> Faculty of Applied Science, Ait Melloul, Ibn Zohr University, Agadir, Morocco

<sup>d</sup> Laboratory of Analytical and Molecular Chemistry/LCAM, Department of Chemistry, Faculty Polydisciplinary Safi, Cadi Ayyad University, Safi, Morocco

<sup>e</sup> College of Pharmacy, Middle East University, Amman, 11831, Jordan

<sup>f</sup> Department of Chemistry, College of Science, Imam Abdulrahman Bin Faisal University, P.O. Box 1982, Dammam 31441, Saudi Arabia

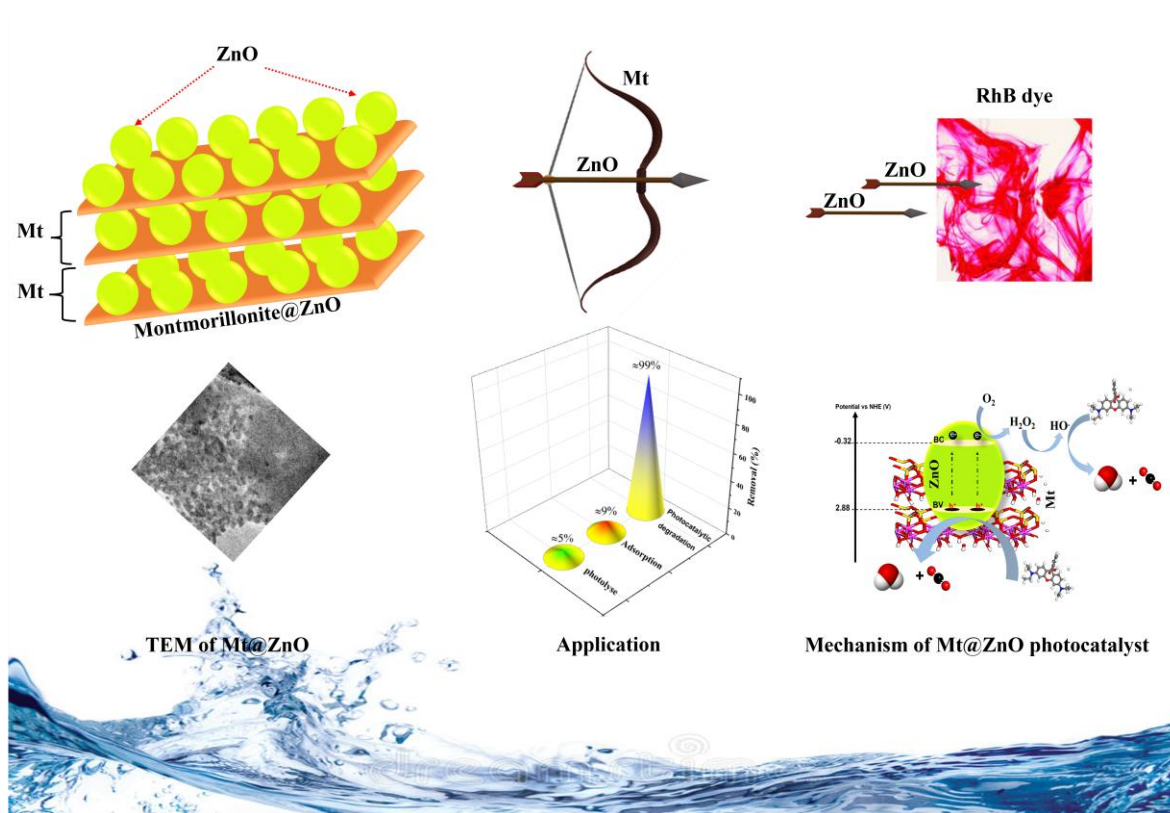
<sup>g</sup> Institute of Materials Science of Mulhouse (IS2M), Haute Alsace University, Mulhouse 68100, France

<sup>h</sup> Strasbourg University, Strasbourg 67081, France

\*Corresponding authors:

[amane.jada@uha.fr](mailto:amane.jada@uha.fr); [ouachtakhassan@gmail.com](mailto:ouachtakhassan@gmail.com); [haounati.redouane@gmail.com](mailto:haounati.redouane@gmail.com)

## Graphical abstract



## Abstract

Photocatalytic degradation of pollutants by nanocomposites is one of the promising approaches to sustainable energy. However, it is difficult for photocatalysts to provide excellent absorption of the photons of light, and at the same time to prevent recombination of the photogenerated electron-hole, and agglomeration of the nanoparticles. Therefore, a catalyst fulfilling these criteria, and supported on clay particles, such as ZnO/Mt nanocomposite was synthesized in the present work by simple co-precipitation approach. The evaluation of the photocatalytic degradation reaction of RhB dye demonstrated that the prepared ZnO/Mt photocatalyst displayed enhanced photocatalytic activity, as compared to pure ZnO. The improved photocatalytic activity of the ZnO/Mt photocatalyst was attributed to the positive synergistic effect occurring between the montmorillonite and the ZnO nanoparticles. Further, theoretical studies were carried out on the RhB dye adsorption on ZnO/Mt. At the first, all used compounds were optimized by DFT-D calculations, the HOMO/LUMO and the total energy were obtained. Then, the molecular dynamic (MD) simulation was used for ZnO adsorption on Montmorillonite (Mt) by using Monte Carlo adsorption locator module. After forming nanocomposite, the adsorption energy of RhB ( $E_{ad}$ ) on ZnO/Mt was applied, suggesting the adsorption process was due to the negative interaction energy. Additionally, the RhB adsorption energy on ZnO/Mt was higher in comparison to the RhB adsorption energy on Mt alone.

**Keywords:** Degradation; Rhodamine B dye; ZnO; Montmorillonite; Molecular dynamic simulations;

## 1. Introduction

Populace relocation, development, extending urbanization, and industrialization over time have impacted the interest in freshwater resources. Modern creation, mining, concentrated agribusiness, and metropolitan utilization have incited an extension in water use, which eventually have remarkably influenced the nature of water open around the planet. Untreated local wastewater and industrial discharges enclose a combination of inorganic and organic pollutants. Thusly, the arrival of wastewater from these places into the ecosystem prompts its pollution[1, 2].

Wastewater the board approaches for the stockpile of safe water is problematic because of the extreme and rapidly creating interest for unpolluted water. Thusly, realization water treatment procedures that are basically highlighted remediating water pollution issues are essential. In this attitude, wastewater treatments systems with high sufficiency need less preparation time and the production of safe bring about water are frantically required. A couple of traditional treatment methods have been used. For instance: biological treatment, membrane separation, chemical precipitation, electrochemical techniques, adsorption, and others [1,3]. However, the aforesaid methods have certain obstacles and drawbacks on the remediation process consisting of high cost operation, ineffectual at low concentration, poor selectivity, and releasing undesirable species into the aquatic environment [4,5].

Organic dyes are comprehensively orchestrated and used in textile and a lot of industrial manufacturing. The inappropriate evacuation of these chemicals compromises the environment and the human health issues [6]. The dyes generally have aromatic structure which makes them stable and non-biodegradable in nature[7]. Moreover, dyes are renowned in toxicity, carcinogenic and mutagenic properties. They have severe damage on liver, brain, kidneys, fertility and nerve system [8]. Rhodamine B (RhB) is a cationic dye that has many uses. Thus, it is used in textile and photographic enterprises and also as a water tracer fluorescent material [9]. Rhodamine B reasons irritation for the eyes, respiratory system and is involved in causing developmental toxicity, reproductive, and neurotoxicity, and chronic toxicity towards animals and human [10].

To deal with issues related to pollution of water and wastewater treatment there are many advanced moves of late in nanotechnology that has supported the utilization of nanomaterials of

the first class. Nanoparticles (NPs) are dimensional materials under 100 nm that show some exceptional chemical and physical perspectives for water treatment. These NPs are used as practical materials in the sorts of metals/oxides, zeolites, dendrimers, and carbonaceous materials [11]. Metal oxide nanoparticles like  $\text{TiO}_2$ ,  $\text{Ag}_2\text{O}$ ,  $\text{ZnO}$ , and  $\text{Fe}_2\text{O}_3$  are active photocatalysts in UV-Vis spectra, nontoxic and biologically inactive, chemically stable and water insoluble and most importantly cost-effective. The inorganic metal oxide,  $\text{ZnO}$ , fills in as a nano adsorbent in view of its non-harmful profile, effective antibacterial movement, and adsorptive properties, mechanical, thermal, and chemical strength [12]. The use of  $\text{ZnO}$  NPs has higher adsorption rates for heavy metals [13]. In addition,  $\text{ZnO}$  NPs show practical choice as photocatalyst for effective degradation of dyes that exist in wastewater. Nevertheless, there are challenges in the huge scope utilization of NPs in water treatment due to: (1) agglomeration of the NPs at high concentrations, (2) higher colloidal stability in aqueous media, and (3) inconvenience in separating and recycling the nanomaterial after use[14]. These limitations can practically be solved by applying certain supports such as clay, glass, activated carbon and natural zeolite [15]. Among various and effective supports, montmorillonite is a suitable candidate due to its high adsorption and cation exchange capacity, interesting structure, abundant and ease of handling[16].

The photodegradation approach is highly concerned in the utilization of NPs for toxic dyes removal from aqueous solutions. However, the major challenges in the processing of these materials for the treatment of wastewater, are related to their post-separation and their recycling after their uses. In view of that, this study reports on using Moroccan natural montmorillonite (Mt), as support material for studying the photodegradation of cationic dye; Rhodamine B dye. Thus,  $\text{ZnO}/\text{Mt}$  nanocomposite was designed and characterized prior its use in the dye photodegradation reactions. Hence, the adsorption equilibrium, the kinetic studies, and the photocatalytic performance in UV-region, were investigated, whereas the effect of  $\text{ZnO}$  NPs on Rhodamine B removal was analyzed with proper mechanism. On the other hand, the quantum chemical calculations and Molecular dynamics (MD) simulations were run to get a deeper understanding of the stable configurations and the elucidate the adsorption mechanisms of RhB dye on  $\text{ZnO}/\text{Mt}$ .

## **2.1. Reagents**

All chemicals in this study are obtained from commercial resources and used as received. Zinc nitrate hexahydrate ( $\text{Zn}(\text{NO}_3)_2 \cdot 6\text{H}_2\text{O}$ , MM 297.49 g mol<sup>-1</sup>, purity 99%), ammonium hydroxide ( $\text{NH}_3\text{OH}$ , MM 35.04 g mol<sup>-1</sup>, 28%), Rhodamine B ( $\text{C}_{28}\text{H}_{31}\text{ClN}_2\text{O}_3$ ; molecular weight: 479.01 g mol<sup>-1</sup>,  $\lambda_{\text{max}} = 554$  nm, Solubility: 1 mg/ml, H<sub>2</sub>O). The origin and the type of montmorillonite (Mt) used in this study was previously published in our recent work[17].

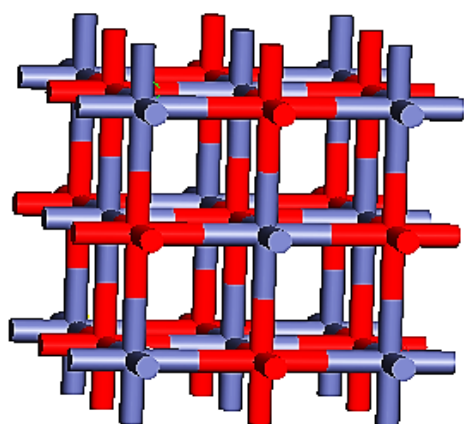
## 2.2. Characterization

The natural clay Montmorillonite and ZnO/Mt nanocomposite were characterized using different characterization techniques. Surface area and type of porosity was performed by Brunauer-Emmett-Teller (BET) method using Quantachrome surface area analyzer. The main functional groups in the range of 4000–400 cm<sup>-1</sup> were allocated by Fourier-transform infrared spectroscopy using IRAFFINTT-2 spectrometer. The XRD of montmorillonite and nano-based composite were recorded by X-ray diffractometer-7000, Shimadzu from 5° to 80° 2 $\theta$  at a scan rate of 2°/min. Scanning electron microscopy (SEM) was applied by INSPECT S50 microscope. Transmission Electron Microscopy TEM (TecnaiG2 12 TWIN) was utilized to fine structures of the photocatalysts. TGA/TDA of samples was acquired by Shimadzu Instruments DTG-60 between 25 and 1000°C (in air, 5°C. min<sup>-1</sup>).

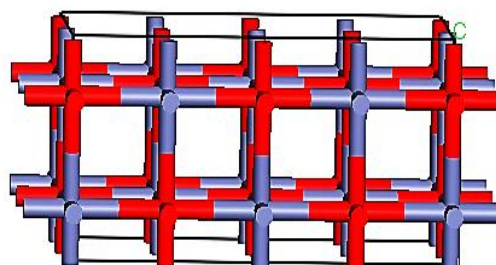
## 2.3. Theoretical calculations

ZnO as Cubic (code; mp-2229, Point Group  $\text{Fm}\bar{3}\text{m}$ ) with  $a = b = c = 4.34$  Å,  $\alpha = \beta = \gamma = 90.000^\circ$  was downloaded from <https://materialsproject.org/materials/mp-2229> (**Figure 1a**), then it was constructed based on (-100) surface and thickness of 1.50 Å (**Figure 1b**) as well as set u v; 1 2, vacuum thickness (0.000) and slab position (1.00) (**Figure 1c**). In addition,  $\text{AlSiO}_5(\text{OH})_4$  (montmorillonite: Mt) as triclinic (ID: mp-541152 and Point Group  $\text{m}\bar{3}\text{m}$ ) with  $a = 5.21$ ,  $b = 7.48$ ,  $c = 9.05$  Å,  $\alpha = 91.79^\circ$ ,  $\beta = 89.73^\circ$ ,  $\gamma = 104.97^\circ$  and volume of 340.74 Å<sup>3</sup> was downloaded from <https://materialsproject.org/materials/mp-541152> [18](**Figure 1d**), then was constructed based on (-100) surface and thickness of 1.574 Å as well as set u v; 2 2, vacuum thickness (0.000) and slab position (1.00) (**Figure 1e**). **Figures 1f** and **1g** are exhibited Mt without unit cell [19,20] RhB and ZnO were optimized through DMol<sup>3</sup> based on DFT-D, the Generalized Gradient Approximation (GGA) / the Perdew–Burke–Ernzerhof (PBE) functional and DND along with spin-unrestricted in Materials Studio 2017 software [21]. At last, Then, 6 ZnO molecules were adsorbed on Mt (-100) by the Monte Carlo adsorption locator module. In

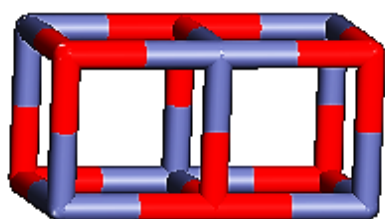
addition, 4 molecules of Rh B were adsorbed on Mt or Mt/ZnO surface the presence of 10 water molecules by the Monte Carlo adsorption locator module to investigate photo-degradation.



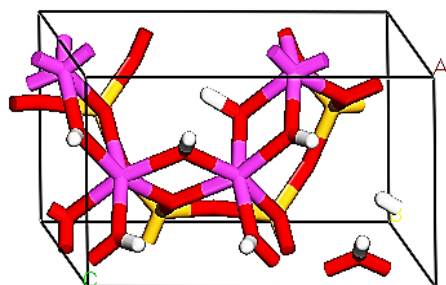
a



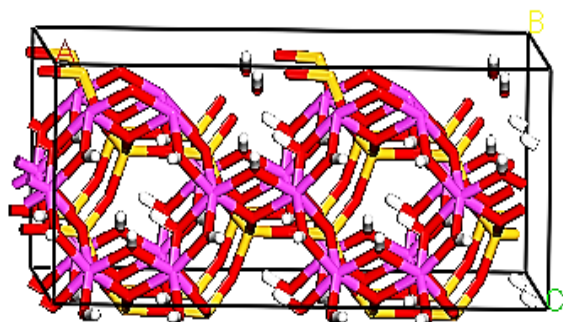
b



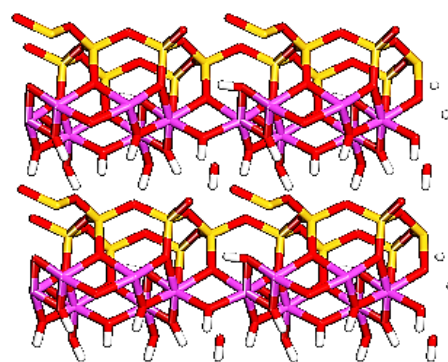
c



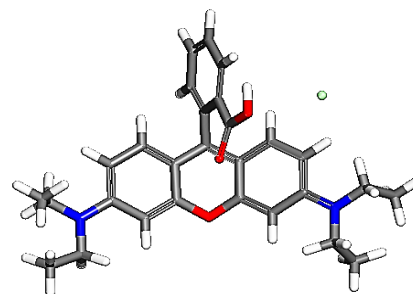
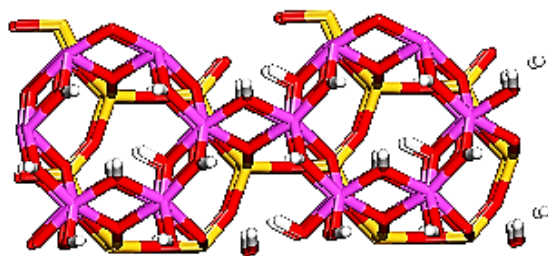
d



e



f



**g** **h**

**Figure 1.** Snapshots of the proposed structures (a-c); ZnO, (d); Mt ((ID: mp-541152), (e); MT based on (-100) surface, (f and g); Top and side views of Mt (-100) and (h); RhB. Colored balls are carbon (grey), oxygen (red), orange (Si), blue (N), pink (Al), light green (Cl), and white (H).

#### 2.4. Preparation of ZnO/Mt composite

The preparation of ZnO modified montmorillonite (ZnO/Mt) was performed by adding 5.0 g of montmorillonite sample into a reaction vessel with 100 mL of 3% ammonia solution. After two hours of sonication, zinc oxide solution (10.0 g of zinc nitrate hexahydrate) was added to the vessel and combined for 2h. Next the system was refluxed for 4h at 100 °C. Then, the mixture was cooled, and the synthesized nanocomposite was gathered by filtration process, and after that it was calcined at 350 °C for 2h

#### 2.5. Photocatalytic degradation experiments of Rhodamine B dye

The photocatalytic efficiency of ZnO/Mt composite material was studied by photodegradation of toxic RhB dye under UV-light. The experiment was done as follows: around 100 mg of ZnO/Mt sample was mixed with 100 mL of RhB aqueous solution with (10 mg/L). Before UV-light irradiation, the system was stirred in the dark for one hour to reach adsorption/ desorption equilibrium between photocatalyst and RhB dye where the initial pH value was fixed at 6. Next, the stirring of the mixed suspension was continued and exposed to irradiation by lamp of xenon (35W) to start the degradation process. At a given time interval (Every 10 min), 2 mL of the suspension was collected from the photocatalytic system and then the remaining RhB concentration was determined using a UV-Vis spectrophotometer (Shimadzu UV-Vis spectrometer) at 554 nm. Finally, the effectiveness of photodegradation was determined with the following equation:

$$\text{Degradation efficiency (\%)} = \frac{(C_0 - C_t)}{C_0} \times 100 \quad \text{Eq. (1)}$$

Whereas  $C_t$  (mg/L) is the dye concentration at time  $t$  and  $C_0$  (mg/L) is the initial dye concentration.

### 3. Results and discussion

#### 3.1 Structure and morphology

The functional grouping of Mt clay and ZnO/Mt nanocomposite were investigated by FTIR spectroscopy (**Figure 2**). The spectra of montmorillonite clay showed that the characteristic band at 447 and 518  $\text{cm}^{-1}$  attributed the deformation modes of Si-O-Si and Al-O-Si respectively [1]. The characteristic bands at 785, 922 and 1047  $\text{cm}^{-1}$  correspond to the deformation vibration mode of Mg-OH, Al-OH and Si-O groups, respectively [22]. Additionally, two large peaks observed at 2441 and 3628  $\text{cm}^{-1}$  can be ascribed to the hydroxide OH related with Al and Si respectively [23]. Notably, for the ZnO/Mt nanocomposite, as can be displayed that the characteristics bands corresponds to the Mt clay shows more than one peak at 454  $\text{cm}^{-1}$  which is attributed the bond vibration Zn-O group [24].

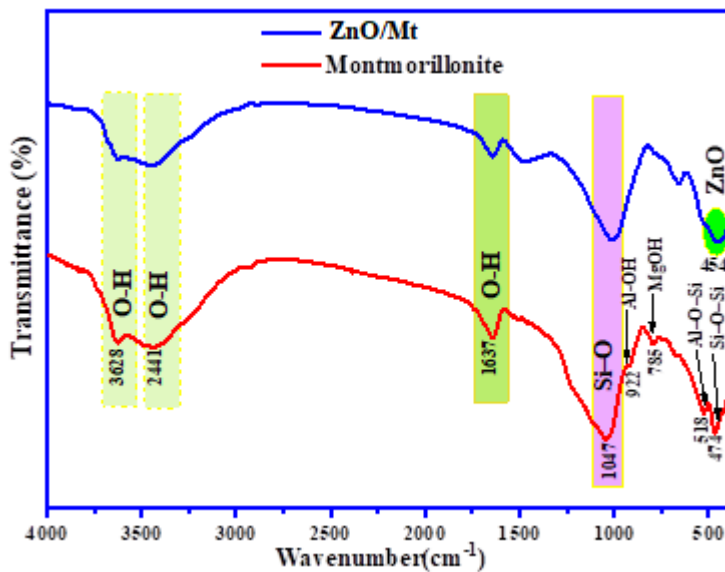


**Figure 2.** FT-IR spectra of ZnO/Mt nanocomposite.

X-ray diffraction is one of the techniques used to investigate the structure of the materials. The X-ray diffraction patterns of samples Mt and Mt modified by ZnO nanoparticles were showed in **Figure 3**. For Mt clay, it can be seen that the main diffraction peaks at  $2\theta = 17.17^\circ$ ,  $19.89^\circ$ ,  $35.02^\circ$ , and  $54.23^\circ$  are consistent with the reflection planes (003), (100), (105), (210) respectively, according to the (JCPDS No. 29-1498) [25]. As can be seen for the XRD pattern of ZnO/Mt nanocomposite, the appearance of the peaks characteristic at  $2\theta$  scale as  $31.77^\circ$ ,  $34.42^\circ$ ,  $36.25^\circ$ ,  $47.53^\circ$  and  $56.60^\circ$  are attributed to the (001), (002), (101), (102), (110) respectively, correspond ZnO Hexagonal wurtzite structure (JCPDS No 036-1451) [26].

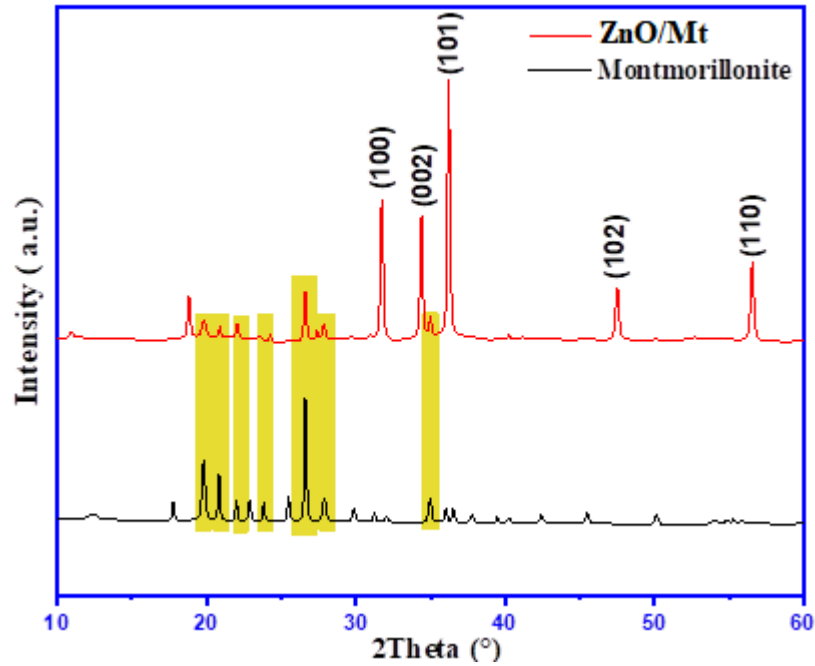


**Figure 3.** X-ray diffraction patterns of Montmorillonite and ZnO/Mt nanocomposite.

The aim of the SEM study is to determine the loading of ZnO on the surface of Montmorillonite. The morphology of ZnO/Mt was studied by SEM. As shown in **Figure 4**, the micrographs (a, b and c) showed that the montmorillonite exhibited a better crystal plate structure. However, the particles of ZnO were uniformly dispersed in the surface of montmorillonite. Thus, the fabricated nanocomposite photocatalysis can be considered as homogeneous, and the clay montmorillonite can be playing a curial role to avoid the agglomerates of the particles of zinc oxide during the photodegradation process.

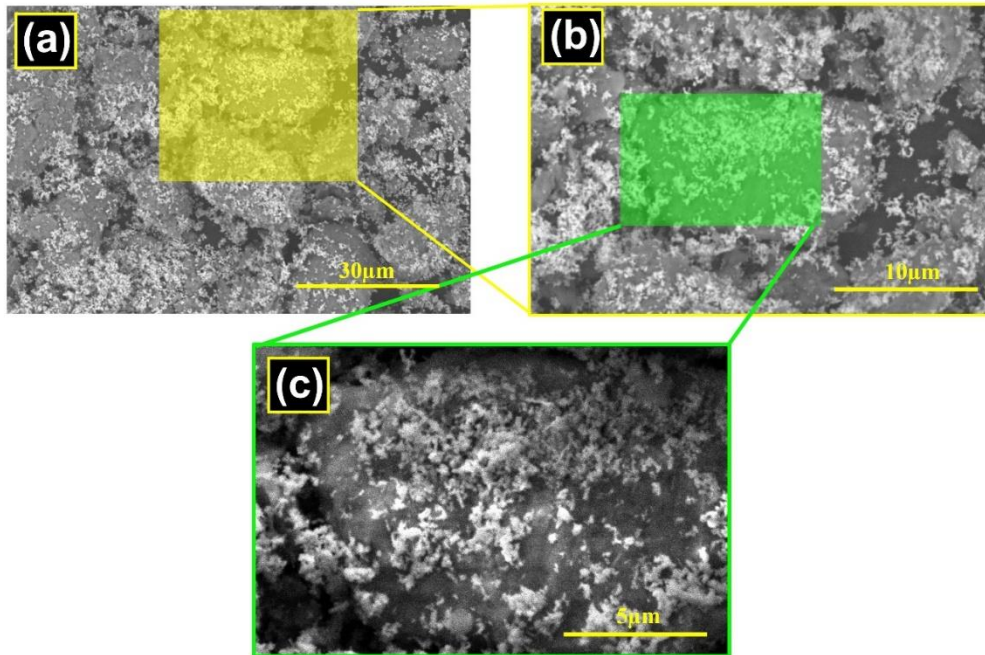


**Figure 4.** SEM images 30  $\mu\text{m}$  (a), 10  $\mu\text{m}$  (b) and 5  $\mu\text{m}$  (c) of ZnO/Mt nanocomposite.

TEM images were provided at different magnifications for the ZnO/Mt nanocomposites. The resulting TEM images are displayed in **Figure 5(a, b, d)** depicting the nanostructured and loaded ZnO nanoparticles on the surface of montmorillonite. The size of the ZnO particles was measured to be about 5-10 nm, as shown in **Figure 5d**.

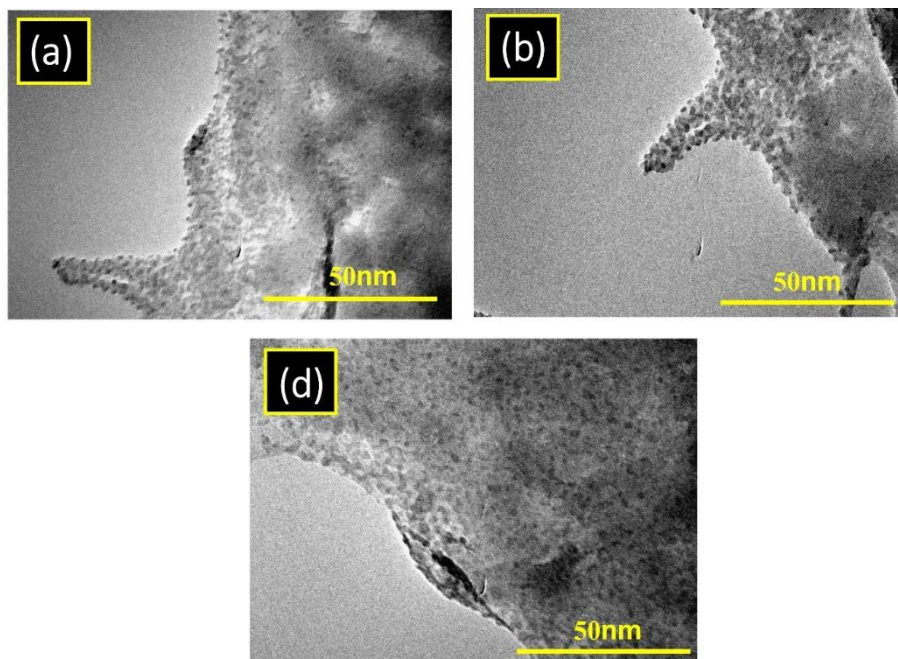


**Figure 5.** TEM images 50 nm of ZnO/Mt nanocomposite.

Thermogravimetric coupling differential thermal analysis (TGA/DTA) was investigated for studying the thermal stability of ZnO/Mt nanocomposite, in a temperature range of 25 °C to 1000 °C, with a heating rate of 5 °C/min (**Figure. 6**) in air environment. The TGA/DTA figure displayed an endothermic phenomena at 90 °C with mass loss of (-1.84 mg), attributed the dehydration i.e. loss of water molecules adsorbed on montmorillonite surface [27]. The observed endothermic peak with a low intensity at 790°C can be associated with dihydroxylation of Mt clay water interlayer.

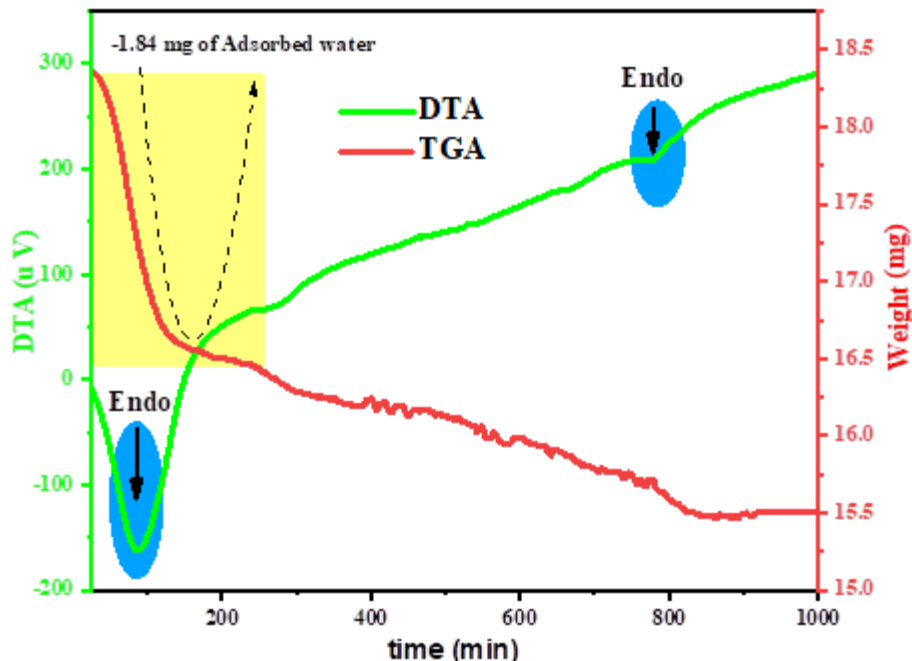


**Figure 6.** Thermograms obtained by TGA/DTA of the ZnO/Mt nanocomposite.

### 3.2 Simulation Methods

#### 3.2.1 Quantum calculations

In order to achieve the most stable configurations and their energies as well as HOMO/LUMO, DMol<sup>3</sup> module, Task: geometry optimization based on GGA/ PBE/DFT-D/DND were used in Materials Studio 2017 (**Figures 7a-c**)[28]. Total Energy of ZnO, Mt and Rh B was obtained -11126.756, -22679.698 and -1880.764, Ha, respectively. The geometric parameters of all compounds are summarized in **Table 1**. HOMO and LUMO orbitals of ZnO were localized on O atoms and Zn, respectively (**Figure 8a**). As showed in **Figure 8b**, HOMO orbitals of Mt (-100) were distributed on almost overall structure, LUMO orbitals of Mt (-100) were distributed the end silicate. HOMO orbitals of Rh B were distributed on all xanthene surfaces; meanwhile, LUMO orbitals of RhB were situated on whole benzoic acid (**Figure 8c**).

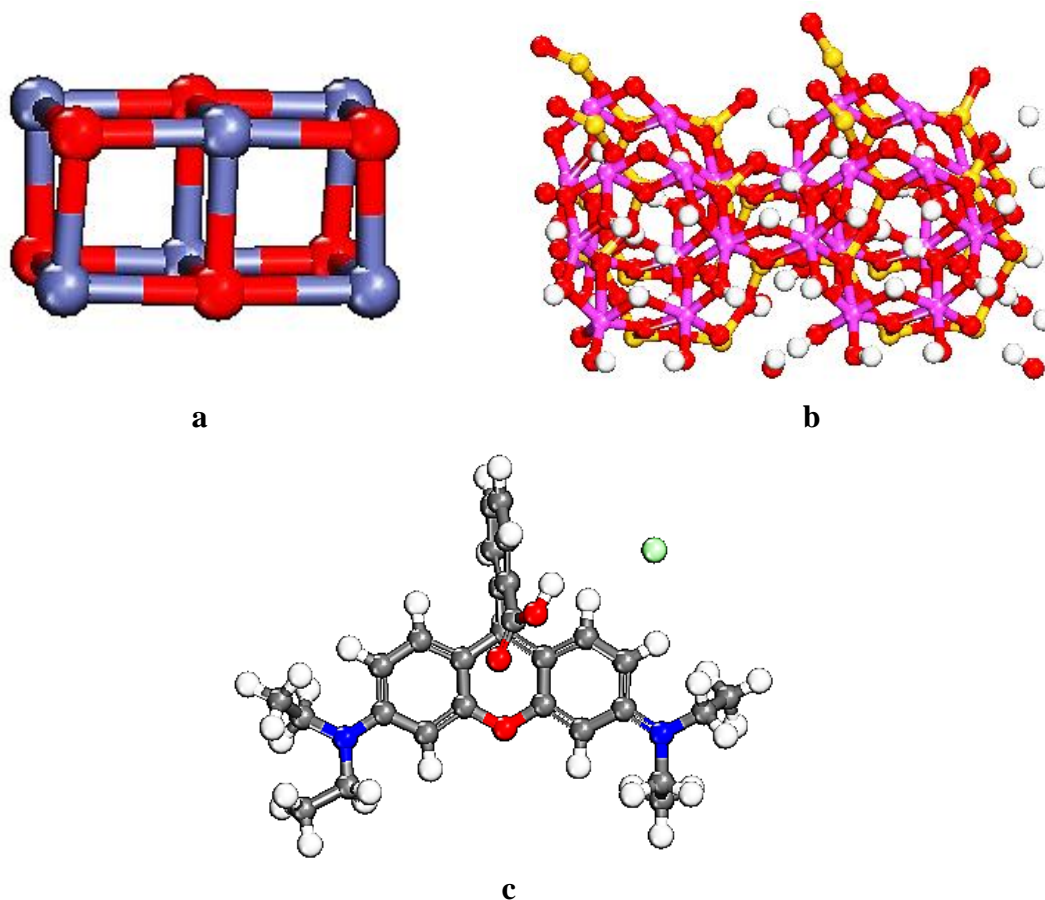


**Figure 7.** DFT-optimized structures resulting (a); ZnO, (b); MT (-100) and (c); Rh B obtained from DMol3 Based on DFT-D.

**Table 1.** The geometric parameters of all compounds obtained by DMol<sup>3</sup> based on DFT-D.

	ZnO	MT	Rh B
<b>Sum of atomic energies</b>	-11125.030	-22635.022	-1868.168
<b>Kinetic</b>	-11.065	-135.117	-18.431
<b>Electrostatic</b>	8.349	63.042	-2.017
<b>Exchange-correlation</b>	0.502	15.730	4.536
<b>Spin polarization</b>	0.510	12.202	3.394
<b>DFT-D correction</b>	-0.023	-0.534	-0.079
<b>Total Energy</b>	-11126.756	-22679.698	-1880.764

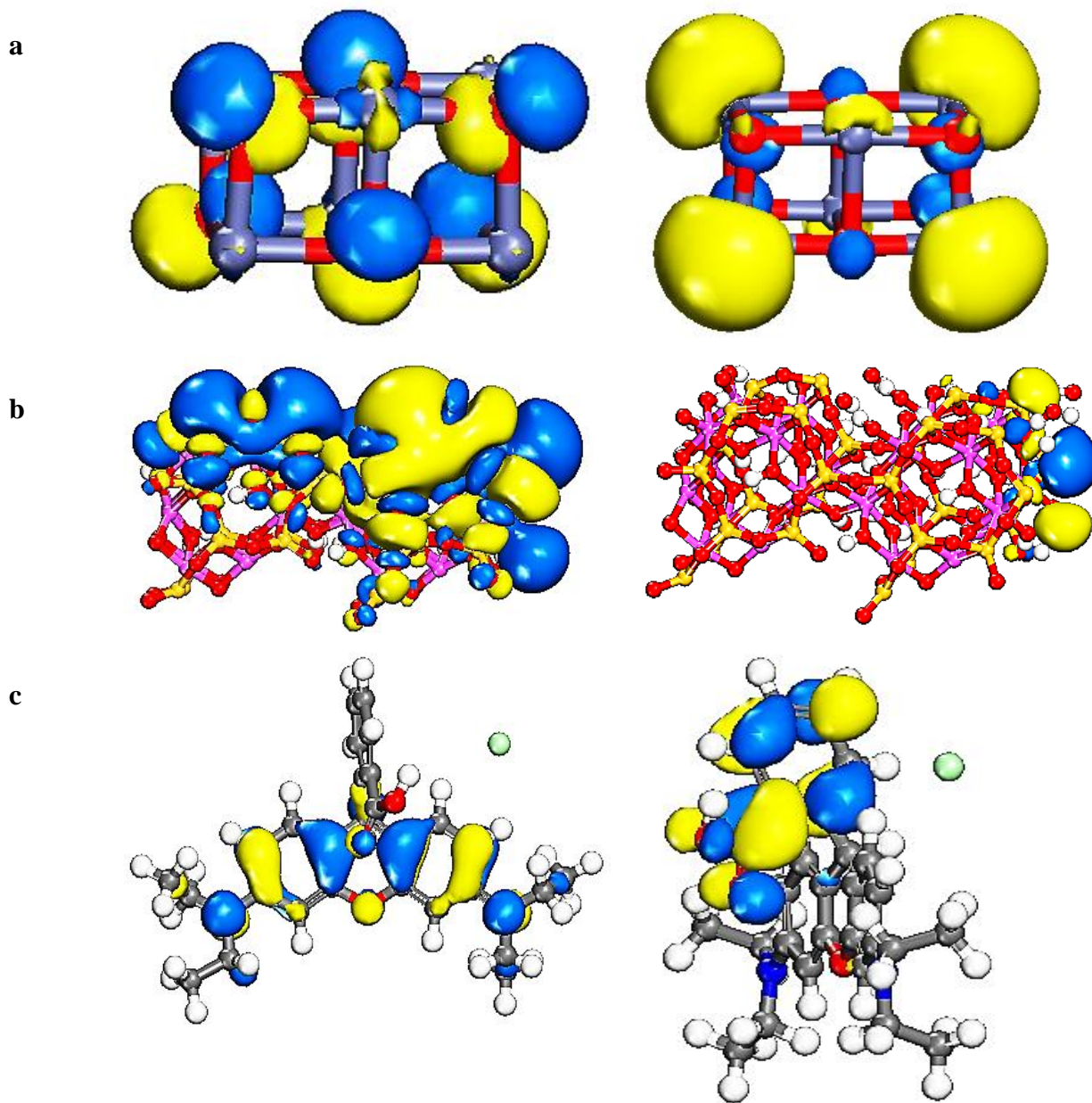


**Figure 8.** Plots of HOMO and LUMO orbital structures of (a); ZnO, (b); Mt and (c); RhB obtained from DMol<sup>3</sup> Based on DFT-D.

### 3.2.2 Modelling by Monte Carlo adsorption locator simulation

After optimization of structures by quantum calculations, the adsorption of 6 ZnO molecules on Mt (-100) was occurred to make ZnO/Mt surface by adsorption locator module and force field; universal in Materials Studio 2017 software (**Figures 9a-b**). The total energy of the system after the adsorption of ZnO ( $E_{ad}$ ) was obtained about  $-2.422 \times 10^3$  kcal/mol, demonstrating the interaction between O atoms of ZnO and silicate groups of Mt (-100) with less than 3 Å.

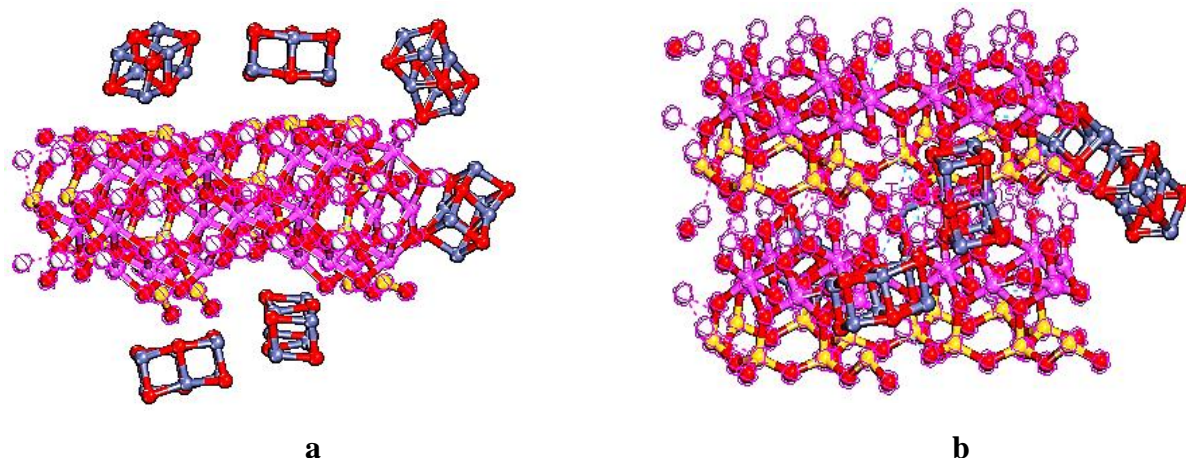


**Figure 9.** (a); Top view and (b); side views of the adsorption of 6 ZnO molecules on Mt (-100) by adsorption locator module in Materials Studio 2017 software

In next stage, ZnO/Mt catalyst was used to adsorb 6 RhB molecules. All the computations were carried out in the aqueous phase. The adsorption energy of RhB ( $E_{ad}$ ) on catalyst by the Monte Carlo adsorption locator module was obtained -414.190 kcal/mol as seen in **Figures 10a-b**. In comparison ZnO/Mt, in order to understand the reactivity of the ZnO/Mt system, MT (-100) was prepared to adsorb 4 molecules of RhB. The adsorption energy ( $E_{ad}$ ) of RhB on Mt (-100) based on MD calculation results was obtained -313.686 kcal/mol as seen in **Figures 10c-d**. The van der Waals force and electrostatic, adsorption mechanisms were incorporated in this studies [29]. RhB was located on the exterior surface of Mt (-100). According to our theoretical results, the interaction energy was negative, which adsorption process demonstrated exothermic and stability of the adsorption system [30,31]. The results showed that RhB be physically adsorbed on the surfaces of the ZnO/Mt and Mt (-100)[32]. It is clear that, the adsorption RhB in ZnO/Mt system was enhanced significantly as compared with Mt (-100), so the reactivity of the ZnO/Mt was increased due to the presence of ZnO. In addition, ZnO can be help in the adsorption of Rh B onto ZnO/Mt composites. So, by adsorbing pollutant on catalyst surface and enhancement of  $e^-$  and  $h^+$  by ZnO and Mt (-100) under UV- light irradiation, Rh B can be degraded by catalyst.

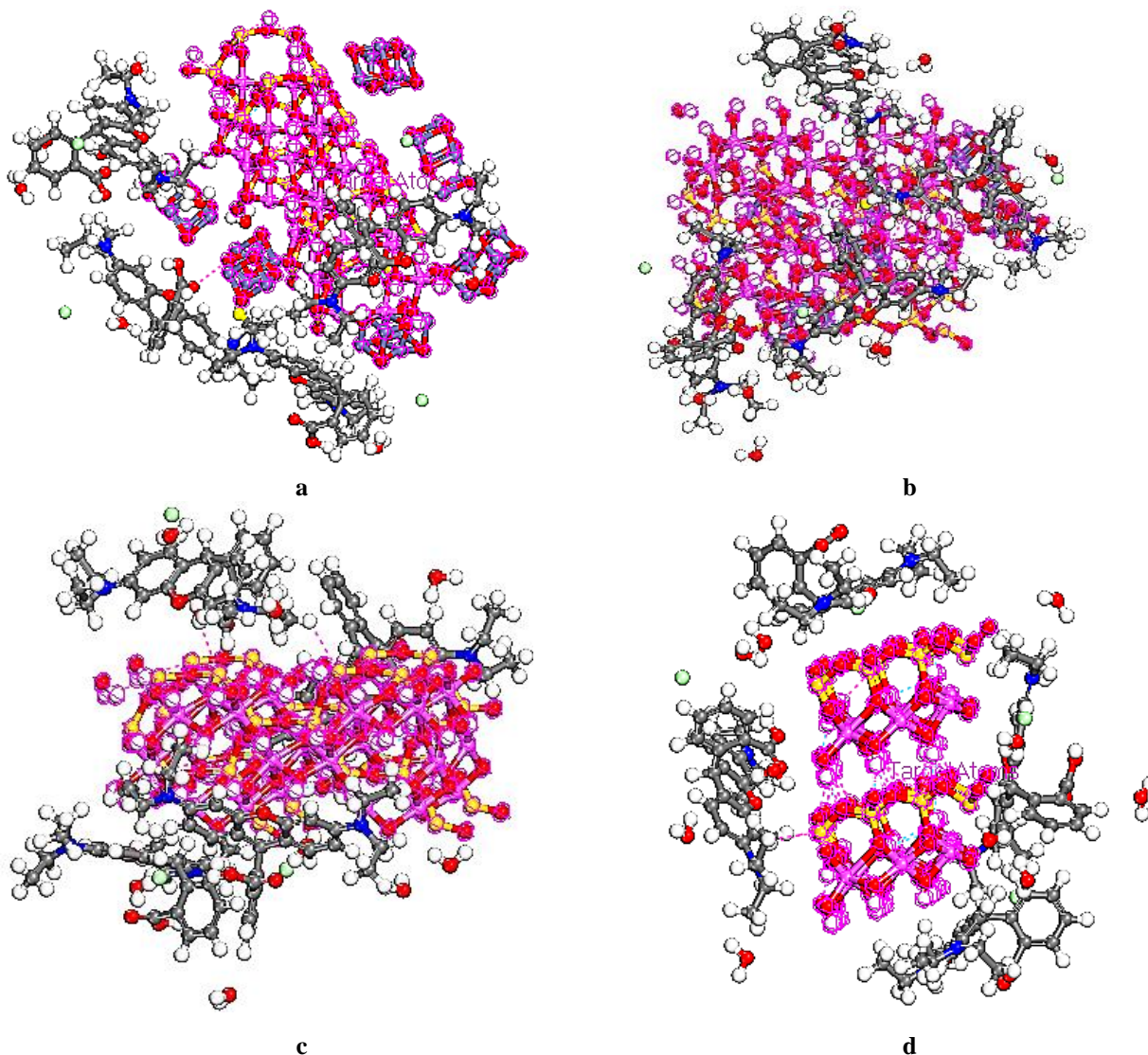


**Figure 10.** (a and b); Top and side views of the adsorption of 4 RhB molecules on ZnO/Mt and (c and d) on MT (-100) by adsorption locator module in Materials Studio 2017 software.

### 3.3 Removal kinetics of RhB from aqueous solutions

Some organic pollutants may be eliminated just by direct photolysis when irradiated with UV-light [33] or without UV-light (adsorption), for this reason it is necessary to confirm this hypothesis for RhB dye. We carried out the elimination of RhB dye in different conditions (i) without ZnO/Mt (ii) in the presence of ZnO/Mt and (iii) in the presence of ZnO/Mt and under UV- light. The results are shown in **Figure 11**, the photolysis efficiency revealed a little reduction in the RhB concentration which was estimated at 5% after 70 min of irradiation, indicating the stability and slow photolysis of RhB.

In the other side, the presence of ZnO/Mt without a UV-light irradiation, was carried before the photocatalytic test **Figure 11**, and the removal efficiency of RhB dye has reached 10%, revealed that the catalyst had the low adsorption activities towards RhB.

We also carried out the irradiation of the RhB dye in the presence of the catalyst ZnO/Mt (**Figure 11**), it is clearly demonstrated that the RhB dye was almost completely degraded with an efficiency of 99%. These results confirmed the photocatalysis nature of the chemical reaction. The ZnO/Mt particles absorbed UV radiation to give rise to highly reactive species, such as hydroxyl radicals ( $\text{HO}^\bullet$ ), which will lead to the RhB dye degradation in solution [34].

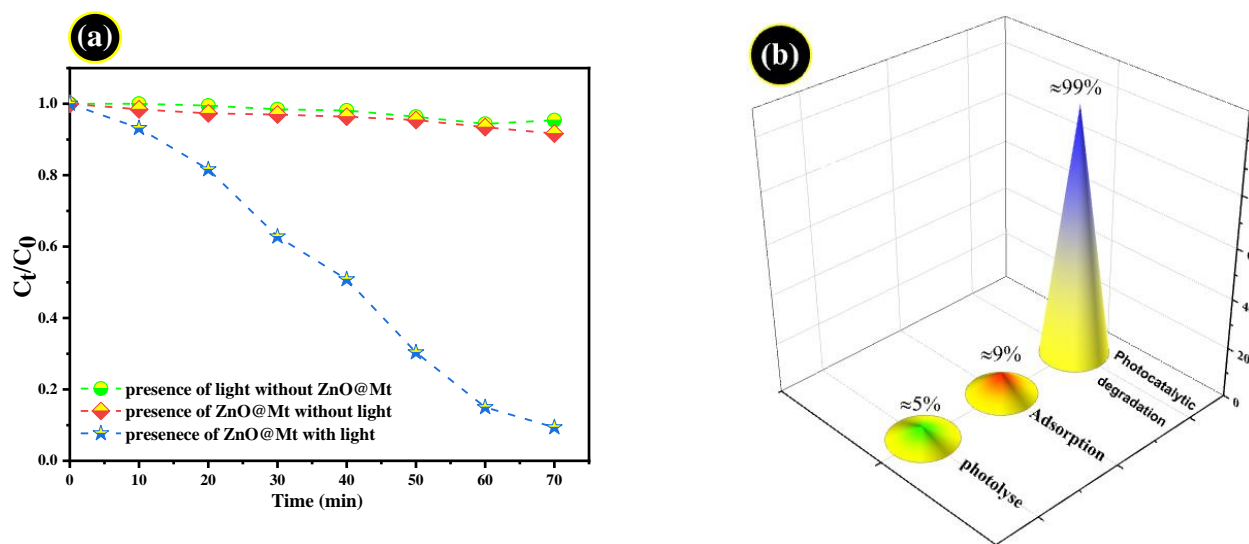


**Figure 11.** Photolysis, adsorption, and photocatalysis of RhB dye on ZnO/Mt

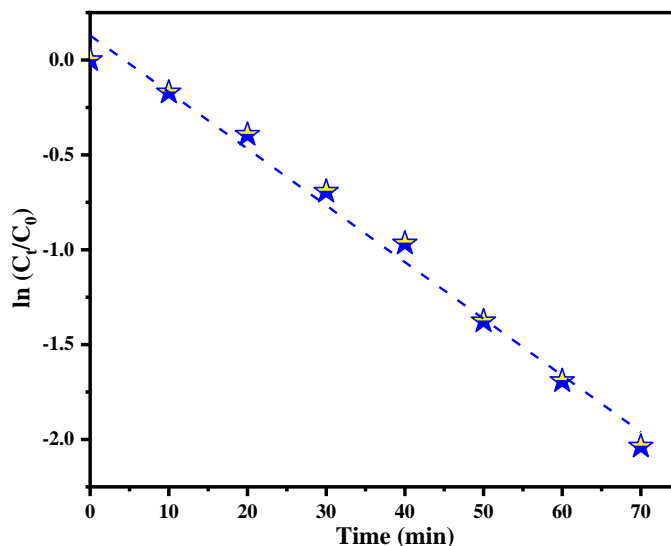


**Figure 12.** Plot of  $\ln(C_t/C_0)$  vs. time (min) for RhB dye in presence of ZnO/Mt nanocrystalline catalyst.

We studied out the kinetics of photocatalytic degradation of RhB dye on the ZnO/Mt composite. The first-order pseudo kinetic plot is displayed in **Figure 12**, and the apparent rate constant  $k_{app}$ , value was obtained using the relation:  $\ln(C_t/C_0) = k_{app}t$

Where  $C_t$  and  $C_0$  ( $\text{mg. L}^{-1}$ ) are the concentration of the dye solution at time  $t$  and initial time, the term  $K_{app}$  denotes the apparent rate constant of dye degradation. The values of the apparent rate constants and half-life times (Eq.3) are given in **Table 2**.

$$t_{1/2} = \ln 2 / k_{app} \quad \text{Eq. 3}$$

**Table 2.** Apparent rate constants ( $k_{app}$ ), linear regression coefficients ( $R^2$ ) and half-life times ( $t_{1/2}$ ) of photocatalytic degradation of RhB.

Initial concentration of RhB ( $\text{mg.L}^{-1}$ )	$t_{1/2}$ (min)	$K_{app}$ ( $10^{-1}.\text{min}^{-1}$ )	$R^2$
10	5.37	0.129	0.99

### 3.4 Stability of the ZnO/Mt photocatalyst

The possibilities of catalyst recovery and its reuse in photocatalytic processes, have been received considerable attention since they can contribute significantly to lowering the operational cost of the process, which is an important parameter in the applicability of photocatalysis as a method for wastewater purification[35]. In order to evaluate stability of photocatalyst, a series of experiments were performed by reusing ZnO/Mt in the photocatalytic reaction under the same condition for four times. The used catalyst was washed with distilled water three times and dried at room temperature during 24 h. As can be seen from **Figure 13**, a little decrease in activity of photocatalytic degradation of RhB was observed after four times of use. Thus, confirmed the stability of the ZnO/Mt in four cycles.

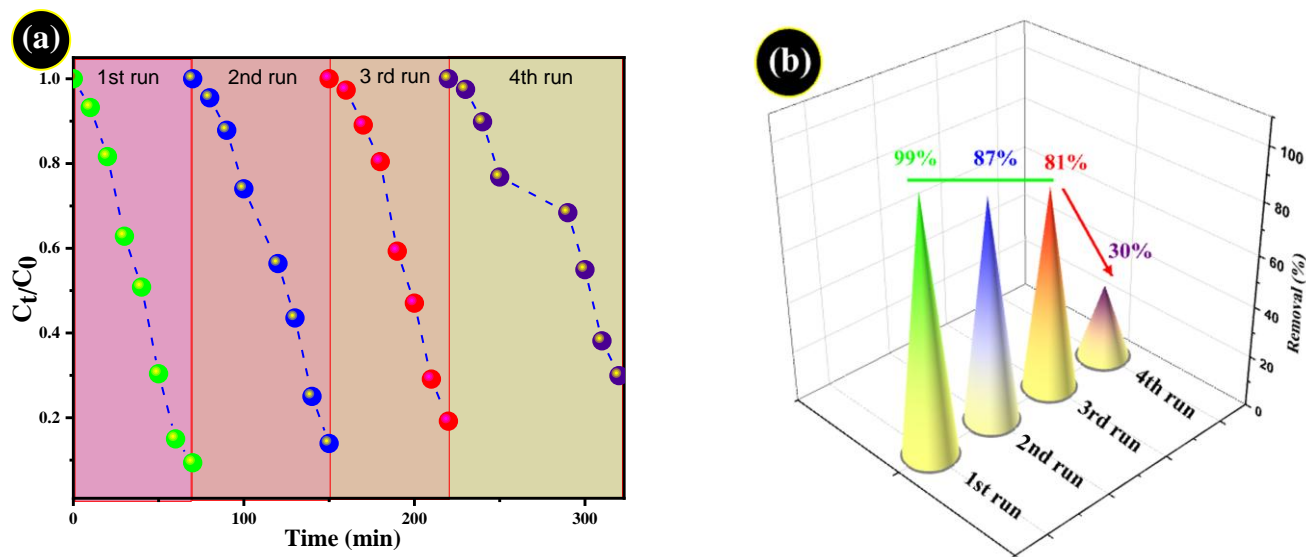


**Figure 13.** Recycling degradation efficiency of ZnO/Mt for RhB

### 3. Dye degradation mechanism by the ZnO/Mt photocatalyst

To highlight the role of the main photoinduced reactive species including hydroxyl radicals ( $\text{HO}^\bullet$ ), holes ( $\text{h}^+$ ), and superoxide radicals ( $\text{O}_2^{\bullet-}$ ) in the photodegradation process, we conducted the photocatalytic tests by adding different trapping amount of organic scavengers (4 mM) including Ethylene Diamine Tetra-acetic Acid EDTA-2Na as  $\text{h}^+$  scavenger, Isopropanol Alcohol (IPA) as  $\text{HO}^\bullet$  scavenger, and L-Ascorbic Acid (ASC) as  $\text{O}_2^{\bullet-}$  scavenger, into the RhB solution before addition of composites catalysts [36].

The results are recorded in **Figure 14**, when no scavenger agent was added, the degradation efficiency of RhB by ZnO/Mt catalyst is about 99%. On the other hand, after the addition EDTA-2Na, IPA, and ASC as the scavenger agent, the degradation efficiency is reduced to 23%, 9% and 74%, respectively. This indicated that both active species  $\text{h}^+$  and  $\text{HO}^\bullet$  played an important role in the photocatalytic degradation of RhB dye. In contrast, it can be observed that  $\text{O}_2^{\bullet-}$  played a little role.

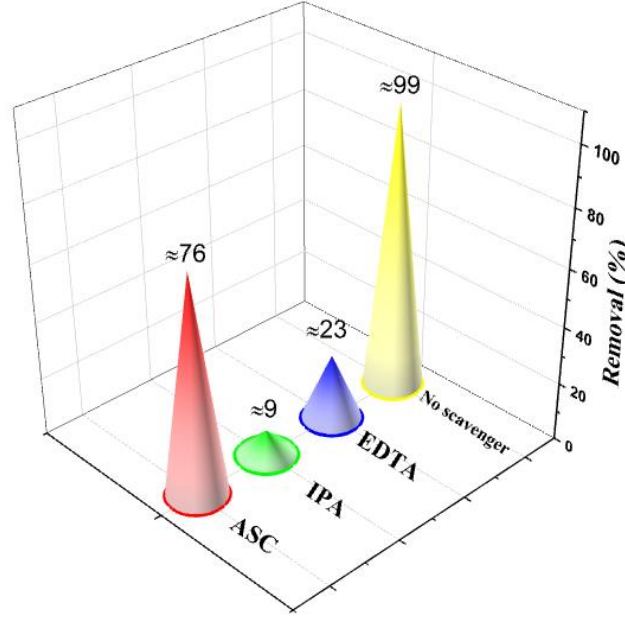


**Figure 14.** Photodegradation of RhB dye over the ZnO/Mt in the presence of different scavenger agents.

The level of the band edge potential is an essential property of semiconductors that determines the process of charge carrier transport and the improvement of the photocatalytic performance. From the literature, the band gap energy of ZnO was found to be 3.21 eV [37]. In addition, the conduction band (CB) edge and valence band (VB) edge potentials of ZnO nanoparticle were determined using the equations of Butler and Ginley's method:

$$\chi_{(ZnO)} = [\chi_{Zn} + \chi_{O}]^{1/2} \quad \text{Eq.4}$$

$$E_{VB} = \chi - E^{\circ} + \frac{E_g}{2} \quad \text{Eq.5}$$

$$E_{CB} = E_{VB} - E_g \quad \text{Eq.6}$$

Where X (ZnO) is the calculated electronegativity of the ZnO semiconductor which is calculated to be 5.78 eV.  $E^{\circ}$  is the free energy of free electron on the hydrogen spectrum (4.5 eV). Based on those values, the  $E_{CB}$  and  $E_{VB}$  of ZnO were determined to be  $-0.32$  and  $+2.88$  eV.

Obviously, the ZnO/Mt nanocomposite with a gap energy equal to 3.21 eV can be excited by UV irradiation. The photogenerated electrons in the valence band can be rapidly transferred to the conduction band of the ZnO nanoparticles, and then the free electrons and holes can be generated in CB and VB, respectively. Moreover, the negative surface of montmorillonite

can play a vital role in the resolution of the problem of electron-hole pair recombination. As can be viewed in Figure 15, the electrons accumulated in the CB of ZnO nanoparticles with a potential of -0.32 eV compared to NHE could be significantly reducing  $O_2$  to produce  $O_2^-$  which is more positive than the standard redox potential of  $O_2/O_2^-$  (- 0.33 eV compared to NHE). Whereas it can react with dissolved  $O_2$  and produce  $H_2O_2$  due to the more positive potential of  $O_2/H_2O_2$  (+ 0.682 eV) and then  $H_2O_2$  can react with electrons to produce HO· radicals. On the other hand, because the CB potential of ZnO is more negative than the potential of  $OH/H_2O$  (~ 2.72 eV), the photogenerated holes cannot react with  $OH^-$  to produce  $OH^-$  but can directly oxidize RhB molecules and produce simple  $CO_2$  and  $H_2O$  molecules.

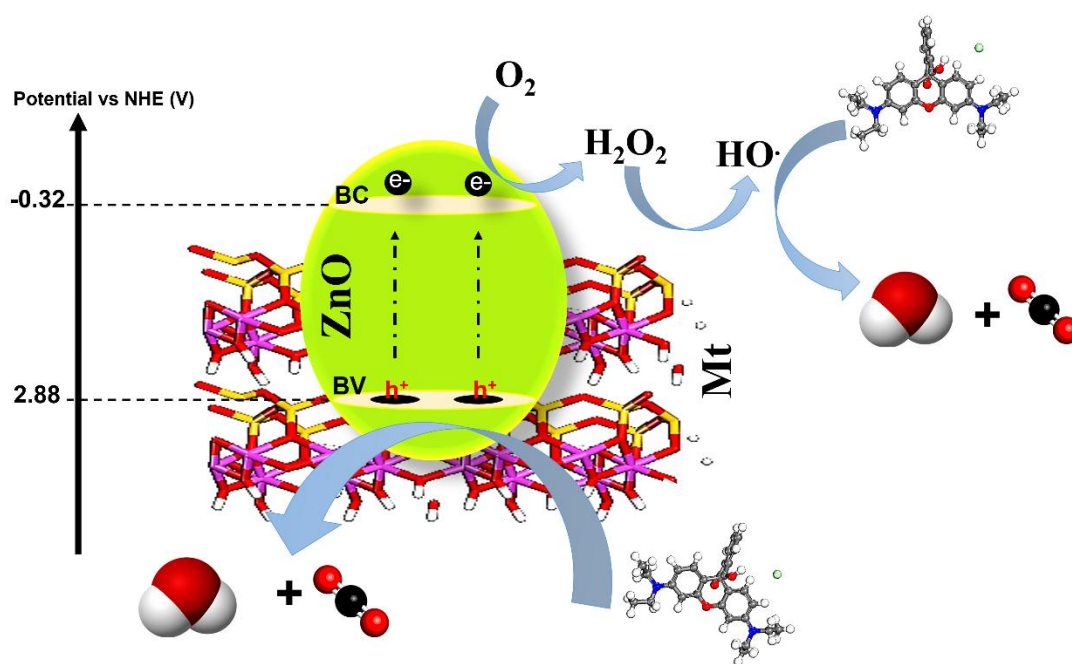


**Figure 15.** Scheme photocatalytic degradation mechanism for RhB over ZnO/Mt nanocomposite.

#### 4. Conclusion

In summary, The ZnO/Mt nanocomposite was synthesized by a simple approach. The prepared nano photocatalyst was characterized using different techniques to evaluate their structural and microstructural properties. Moreover, the photodegradation of RhB dye was studied on ZnO/Mt nanocomposite. In comparison with pure ZnO, the photocatalyst nanocomposite ZnO/Mt was found to exhibit significantly improved photocatalytic activity for the organic pollutant RhB degradation, under UV-light irradiation. It was observed that

the produced HO<sup>•</sup> radicals and h<sup>+</sup> holes play important contributions to the photocatalytic RhB dye degradation. Furthermore, the ZnO/Mt nanocomposite sample could effectively degrade hazardous organic pollutions under UV light and demonstrate the strong potential of application on environmental management. The DFT calculations and The MD simulations were also assumed in this study. After fully structural optimization of all compounds as the most stable configurations by DFT-D calculations, Monte Carlo adsorption locator module was used for ZnO adsorption on Mt, demonstrating high reactivity and strong interactions. At last, MD simulation was applied to adsorb cationic dye (RhB) on Mt and ZnO/Mt. The overall data showed higher physical RhB adsorption on ZnO/Mt in comparison to Mt. In addition, E<sub>ad</sub> of all stages were found to be negative, indicating exothermic adsorption and stability of the adsorption system.

## References

- [1] R. Haounati, H. Ouachtak, R. El Haouti, S. Akhouairi, F. Largo, F. Akbal, A. Benlhachemi, A. Jada, A. Ait Addi, Elaboration and properties of a new SDS / CTAB @ Montmorillonite organoclay composite as a superb adsorbent for the removal of malachite green from aqueous solutions, *Sep. Purif. Technol.* 255 (2021) 117335. <https://doi.org/10.1016/j.seppur.2020.117335>.
- [2] R. Haounati, A. El Guerdaoui, H. Ouachtak, R. El Haouti, A. Bouddouch, N. Hafid, B. Bakiz, D.M.F. Santos, M. Labd Taha, A. Jada, A. Ait Addi, Design of direct Z-scheme superb magnetic nanocomposite photocatalyst Fe<sub>3</sub>O<sub>4</sub>/Ag<sub>3</sub>PO<sub>4</sub>@Sep for hazardous dye degradation, *Sep. Purif. Technol.* 277 (2021) 119399. <https://doi.org/10.1016/j.seppur.2021.119399>.

- [3] E. Al Abbad, F. Alakhras, Removal of Dye Acid Red 1 from Aqueous Solutions Using Chitosan-iso-Vanillin Sorbent Material, *Indones. J. Sci. Technol.* 5 (2020) 352–365. <https://doi.org/10.17509/ijost.v5i3.24986>.
- [4] O. Assila, M. Zouheir, K. Tanji, R. Haounati, F. Zerrouq, A. Kherbeche, Copper nickel co-impregnation of Moroccan yellow clay as promising catalysts for the catalytic wet peroxide oxidation of caffeine, *Heliyon.* 7 (2021) e06069.
- [5] R. El Haouti, H. Ouachtak, A. El Guerdaoui, A. Amedlous, E. Amaterz, R. Haounati, A.A. Addi, F. Akbal, N. El Alem, M.L. Taha, Cationic dyes adsorption by Na-Montmorillonite Nano Clay: Experimental study combined with a theoretical investigation using DFT-based descriptors and molecular dynamics simulations, *J. Mol. Liq.* 290 (2019). <https://doi.org/10.1016/j.molliq.2019.111139>.
- [6] R. Zhu, Q. Chen, Q. Zhou, Y. Xi, J. Zhu, H. He, Adsorbents based on montmorillonite for contaminant removal from water: A review, *Appl. Clay Sci.* 123 (2016) 239–258. <https://doi.org/10.1016/j.clay.2015.12.024>.
- [7] L. Bulgariu, L.B. Escudero, O.S. Bello, M. Iqbal, J. Nisar, K.A. Adegoke, F. Alakhras, M. Kornaros, I. Anastopoulos, The utilization of leaf-based adsorbents for dyes removal: A review, *J. Mol. Liq.* 276 (2019) 728–747.
- [8] B.G. Shen, J.R. Sun, F.X. Hu, H.W. Zhang, Z.H. Cheng, Recent Progress in Exploring Magnetocaloric Materials, *Adv. Mater.* 21 (2009) 4545–4564. <https://doi.org/10.1002/adma.200901072>.
- [9] J. Guo, L. Si, Y. Kong, K.T. Flaherty, X. Xu, Y. Zhu, C.L. Corless, L. Li, H. Li, X. Sheng, C. Cui, Z. Chi, S. Li, M. Han, L. Mao, X. Lin, N. Du, X. Zhang, J. Li, B. Wang, S. Qin, Phase II, Open-Label, Single-Arm Trial of Imatinib Mesylate in Patients With Metastatic Melanoma Harboring *c-Kit* Mutation or Amplification, *J. Clin. Oncol.* 29 (2011) 2904–2909. <https://doi.org/10.1200/JCO.2010.33.9275>.
- [10] R. Nagaraja, N. Kottam, C.R. Girija, B.M. Nagabhushana, Photocatalytic degradation of Rhodamine B dye under UV/solar light using ZnO nanopowder synthesized by solution combustion route, *Powder Technol.* 215–216 (2012) 91–97. <https://doi.org/10.1016/j.powtec.2011.09.014>.
- [11] S. Mustapha, M.M. Ndamitso, A.S. Abdulkareem, J.O. Tijani, D.T. Shuaib, A.O. Ajala, A.K. Mohammed, Application of TiO<sub>2</sub> and ZnO nanoparticles immobilized on clay in wastewater treatment: a review, *Appl. Water Sci.* 10 (2020) 49. <https://doi.org/10.1007/s13201-019-1138-y>.

- [12] M.M. Ibrahim, S. Asal, Physicochemical and photocatalytic studies of  $\text{Ln}^{3+}$ - ZnO for water disinfection and wastewater treatment applications, *J. Mol. Struct.* 1149 (2017) 404–413. <https://doi.org/10.1016/j.molstruc.2017.08.007>.
- [13] M.T. Rafiq, R. Aziz, X. Yang, W. Xiao, M.K. Rafiq, B. Ali, T. Li, Cadmium phytoavailability to rice (*Oryza sativa* L.) grown in representative Chinese soils. A model to improve soil environmental quality guidelines for food safety, *Ecotoxicol. Environ. Saf.* 103 (2014) 101–107. <https://doi.org/10.1016/j.ecoenv.2013.10.016>.
- [14] F. Petronella, A. Truppi, C. Ingrosso, T. Placido, M. Striccoli, M.L. Curri, A. Agostiano, R. Comparelli, Nanocomposite materials for photocatalytic degradation of pollutants, *Catal. Today*. 281 (2017) 85–100. <https://doi.org/10.1016/j.cattod.2016.05.048>.
- [15] F. Alakhras, E. Alhajri, R. Haounati, H. Ouachtak, A.A. Addi, T.A. Saleh, A comparative study of photocatalytic degradation of Rhodamine B using natural-based zeolite composites, *Surfaces and Interfaces*. 20 (2020) 100611. <https://doi.org/10.1016/j.surfin.2020.100611>.
- [16] H.A. Sani, M.B. Ahmad, M.Z. Hussein, N.A. Ibrahim, A. Musa, T.A. Saleh, Nanocomposite of ZnO with montmorillonite for removal of lead and copper ions from aqueous solutions, *Process Saf. Environ. Prot.* 109 (2017) 97–105. <https://doi.org/10.1016/j.psep.2017.03.024>.
- [17] H. Ouachtak, R. El Haouti, A. El Guerdaoui, R. Haounati, E. Amaterz, A.A. Addi, F. Akbal, M.L. Taha, Experimental and molecular dynamics simulation study on the adsorption of Rhodamine B dye on magnetic montmorillonite composite  $\gamma\text{-Fe}_2\text{O}_3\text{@Mt}$ , *J. Mol. Liq.* 309 (2020) 113142. <https://doi.org/10.1016/j.molliq.2020.113142>.
- [18] C. Peng, F. Min, L. Liu, J. Chen, A periodic DFT study of adsorption of water on sodium-montmorillonite (001) basal and (010) edge surface, *Appl. Surf. Sci.* 387 (2016) 308–316. <https://doi.org/10.1016/j.apsusc.2016.06.079>.
- [19] A.R. Akbarzadeh, I. Mesgarzadeh, R. Eshaghi Malekshah, Solution-phase polyol synthesis and coadsorption MD calculations from faceted platinum nanoparticles: NOVEL NPs–polymer morphology controlling, *Chem. Pap.* 76 (2022) 5761–5774. <https://doi.org/10.1007/s11696-022-02272-3>.
- [20] Z. Heidari, R. Pelalak, R. Eshaghi Malekshah, M. Pishnamazi, M. Rezakazemi, T.M. Aminabhavi, S. Shirazian, A new insight into catalytic ozonation of sulfasalazine antibiotic by plasma-treated limonite nanostructures: Experimental, modeling and mechanism, *Chem. Eng. J.* 428 (2022) 131230. <https://doi.org/10.1016/j.cej.2021.131230>.

- [21] Z. Heidari, R. Pelalak, R.E. Malekshah, M. Pishnamazi, A. Marjani, S.M. Sarkar, S. Shirazian, Molecular modeling investigation on mechanism of cationic dyes removal from aqueous solutions by mesoporous materials, *J. Mol. Liq.* 329 (2021) 115485. <https://doi.org/10.1016/j.molliq.2021.115485>.
- [22] H. Ouachtak, A. El Guerdaoui, R. Haounati, S. Akhouairi, R. El Haouti, N. Hafid, A. Ait Addi, B. Šljukić, D.M.F. Santos, M.L. Taha, Highly efficient and fast batch adsorption of orange G dye from polluted water using superb organo-montmorillonite: Experimental study and molecular dynamics investigation, *J. Mol. Liq.* 335 (2021) 116560. <https://doi.org/10.1016/j.molliq.2021.116560>.
- [23] X. Qi, Q. Zeng, X. Tong, T. Su, L. Xie, K. Yuan, J. Xu, J. Shen, Polydopamine/montmorillonite-embedded pullulan hydrogels as efficient adsorbents for removing crystal violet, *J. Hazard. Mater.* 402 (2021) 123359. <https://doi.org/10.1016/j.jhazmat.2020.123359>.
- [24] S. Kumar, S. Kumar, R.D. Kaushik, L.P. Purohit, ZnO-CdO nanocomposites incorporated with graphene oxide nanosheets for efficient photocatalytic degradation of bisphenol A , thymol blue and ciprofloxacin, *J. Hazard. Mater.* 424 (2022) 127332. <https://doi.org/10.1016/j.jhazmat.2021.127332>.
- [25] J. Chang, J. Ma, Q. Ma, D. Zhang, N. Qiao, M. Hu, H. Ma, Adsorption of methylene blue onto Fe<sub>3</sub>O<sub>4</sub>/activated montmorillonite nanocomposite, *Appl. Clay Sci.* 119 (2016) 132–140. <https://doi.org/10.1016/j.clay.2015.06.038>.
- [26] H. Chen, S. Wageh, A.A. Al-Ghamdi, H. Wang, J. Yu, C. Jiang, Hierarchical C/NiO-ZnO nanocomposite fibers with enhanced adsorption capacity for Congo red, *J. Colloid Interface Sci.* 537 (2019) 736–745. <https://doi.org/10.1016/j.jcis.2018.11.045>.
- [27] M. del Mar Orta, J. Martín, S. Medina-Carrasco, J.L. Santos, I. Aparicio, E. Alonso, Adsorption of propranolol onto montmorillonite: Kinetic, isotherm and pH studies, *Appl. Clay Sci.* 173 (2019) 107–114. <https://doi.org/10.1016/j.clay.2019.03.015>.
- [28] K. Gholivand, S.A. Alavinasab Ardebili, M. Mohammadpour, R. Eshaghi Malekshah, S. Hasannia, B. Onagh, Preparation and examination of a scaffold based on hydroxylated polyphosphazene for tissue engineering: In vitro and in vivo studies, *J. Appl. Polym. Sci.* 139 (2022) 1–19. <https://doi.org/10.1002/app.52179>.
- [29] R. Alvand, M. Rezaei-Sameti, The H<sup>+</sup> ions and static electric field effects on the adsorption and detection of cyanogen fluoride on the surface of boron nitride nanocage: a DFT, TD-DFT study, *Adsorption.* 27 (2021) 91–104. <https://doi.org/10.1007/s10450-020-00278-5>.

- [30] Y. Zhu, B. Luo, C. Sun, J. Liu, H. Sun, Y. Li, Y. Han, Density functional theory study of  $\alpha$ -Bromolauric acid adsorption on the  $\alpha$ -quartz (1 0 1) surface, *Miner. Eng.* 92 (2016) 72–77. <https://doi.org/10.1016/j.mineng.2016.03.007>.
- [31] M. Kamel, H. Raissi, A. Morsali, M. Shahabi, Assessment of the adsorption mechanism of Flutamide anticancer drug on the functionalized single-walled carbon nanotube surface as a drug delivery vehicle: An alternative theoretical approach based on DFT and MD, *Appl. Surf. Sci.* 434 (2018) 492–503. <https://doi.org/10.1016/j.apsusc.2017.10.165>.
- [32] B. Fahimirad, R.E. Malekshah, M.A. Chamjangali, R.K. Abasabadi, S. Bromand, Theoretical and experimental study of the photodegradation of methyl orange in the presence of different morphologies of Au-ZnO using Monte Carlo dynamic simulation, *Environ. Sci. Pollut. Res.* (2022). <https://doi.org/10.1007/s11356-022-19657-2>.
- [33] E.H. Mourid, E.M. El Mouchtari, L. El Mersly, L. Benaziz, S. Rafqah, M. Lakraimi, Development of a new recyclable nanocomposite LDH-TiO<sub>2</sub> for the degradation of antibiotic sulfamethoxazole under UVA radiation: An approach towards sunlight, *J. Photochem. Photobiol. A Chem.* 396 (2020) 112530. <https://doi.org/10.1016/j.jphotochem.2020.112530>.
- [34] S. Alahiane, A. Sennaoui, F. Sakr, M. Dinne, S. Qourzal, A. Assabbane, Synchronous role of coupled adsorption-photocatalytic degradation of Direct Red 80 with nanocrystalline TiO<sub>2</sub>-coated non-woven fibres materials in a static batch photoreactor, *Groundw. Sustain. Dev.* 11 (2020) 100396. <https://doi.org/10.1016/j.gsd.2020.100396>.
- [35] R. Haounati, F. Alakhras, H. Ouachtak, T.A. Saleh, G. Al-Mazaideh, E. Alhajri, A. Jada, N. Hafid, A.A. Addi, Synthesized of Zeolite@Ag<sub>2</sub>O Nanocomposite as Superb Stability Photocatalysis Toward Hazardous Rhodamine B Dye from Water, *Arab. J. Sci. Eng.* (2022). <https://doi.org/10.1007/s13369-022-06899-y>.
- [36] H.J. Jung, D. Kim, S. Kim, J. Park, V.P. Dravid, B. Shin, Stability of Halide Perovskite Solar Cell Devices: In Situ Observation of Oxygen Diffusion under Biasing, *Adv. Mater.* 30 (2018) 1802769. <https://doi.org/10.1002/adma.201802769>.
- [37] R. Abdel-Aziz, M.A. Ahmed, M.F. Abdel-Messih, A novel UV and visible light driven photocatalyst AgIO<sub>4</sub>/ZnO nanoparticles with highly enhanced photocatalytic performance for removal of rhodamine B and indigo carmine dyes, *J. Photochem. Photobiol. A Chem.* 389 (2020) 112245. <https://doi.org/10.1016/j.jphotochem.2019.112245>.

